Analysis of Flamelet Leading Point Dynamics in an Inhomogeneous Flow

A. Amato[1]   *T. Lieuwen*[1]

[1]*School of Aerospace and Mechanical Engineering, Georgia Institute of Technology, Atlanta, GA, 30332, USA*

Several studies have utilized "leading points" concepts to explain the augmentation of burning rates in turbulent flames by flow fluctuations. These ideas have been particularly utilized to explain the strong sensitivity of the burning rate to fuel composition. Leading point concepts suggest that the burning velocity is controlled by the velocity of the points on the flame that propagate farthest out into the reactants - thus, they de-emphasize the classical idea that burning velocity enhancement is due to increases in flame surface area. Rather, within this interpretation, flame area creation is the effect, not the cause, of augmented turbulent burning velocities. However, the theory behind the implementation of leading point concepts in turbulent combustion modeling needs further development and the definition of "leading point" has not been fully clarified. For a certain class of steady shear flows, it is straightforward to demonstrate the leading point concept in an intuitive manner, but the problem becomes more complex when the leading points themselves evolve in time. In this paper, we use the G-equation to describe the flame dynamics and, utilizing results for Hamilton-Jacobi equations from the Aubry-Mather theory, show how the large-time behavior of its solutions under certain conditions is controlled only by discrete points on the flame, whose space-time evolution in characteristic space forms a set of "optimal characteristics". However, it is possible to find other conditions where the large time behavior of the flame is not controlled by discrete points on the flame, but rather by its entire surface. Moreover, we also show that even in cases where the burning rate is controlled by discrete points, these points are not necessarily the most forward lying points in the flame front. Finally, we consider the case where the laminar flame speed is a weak function of flame curvature and derive exact results for the sensitivity of the front speed to the Markstein length, ℓ, for $\ell > 0$. These solutions explicitly illustrate the reduction of front displacement speed for increasing ℓ, a result previously suggested by measurements.

1. Introduction

The propagation of premixed flames in turbulent flows is a problem of wide practical interest, with a significant literature on their propagation speed, consumption rate, and front topology. While certain scalings and parametric dependencies are well understood, a variety of problems remain [9]. For example, it is well known that fuel/oxidizer composition has a strong influence on turbulent burning rates [34]. However, the understanding and modeling of these effects is still in its infancy [15]. Similarly, the extent to which the turbulent burning rate exhibits a "bending" or saturation at high turbulence intensities is still not well understood.

Classical explanations for augmentation of turbulent burning rates of premixed flames by turbulent velocity fluctuations rely on "global" arguments relating to flame area [13] - i.e., in constant burning velocity flames, the turbulent burning velocity increase is directly proportional to the increase in flame surface area. A key goal of modeling approaches within this framework is to scale the dependence of the surface area weighted burning rate upon turbulence intensity and scale size. An alternative approach to understand turbulent augmentation of burning rates is based upon so-called "leading points", which are intrinsically *local* properties of the turbulent flame. This concept was originally proposed by Zeldovich [55], who described the "leading/pilot" points as the most forward-lying points of the flame front in the direction of the reactants. This idea was subsequently expanded on in a number of references [31, 34]. In a turbulent premixed flame, the largest velocity fluctuations in the direction of propagation create convex bulges with respect to the reactants which generate flame surface area behind them and determine the average combustion velocity. Thus, leading points are loosely defined as positively curved points on the turbulent flame front that propagate out

furthest into the reactants in spatial regions where turbulent eddies induce low approach flow velocities. Within this interpretation, *augmentation of flame surface area is the effect of increased burning rates, not the fundamental cause*.

This concept has been invoked by several investigators to explain the effect of fuel/oxidizer composition on turbulent burning rates of premixed flames [34, 46, 48]. In the leading point concept framework it is postulated that the modifications in the overall turbulent combustion speed depend solely on modification of the burning rate at the leading points since an increase (decrease) in the average propagation speed of this points causes more (less) flame area to be produced behind them. Modeling of turbulent burning rates by leading point concept, then, can be thought as consisting of two sub-problems: the modeling of burning rates at the leading points and the modeling of the dynamics/statistics of the leading points in the turbulent flame. The first problem has been treated previously by modeling the burning rate of the leading point using results derived from canonical geometries, such as quasi-steady "critically" stretched flamelet [3] (stationary curved flame ball [2], expanding spherical flames of small radius [27, 32] and planar, steady opposed-flow twin flames near extinction [31, 46, 48]) or by an empirical formula based on some "effective" Lewis number of the mixture [14, 38, 39].

Turning to the second problem – modeling the dynamics of the leading point itself – few results are available, mainly because the basic leading point argument itself is somewhat phenomenological and remains to be put on firm theoretical footing. There are two instances where the leading points concept can be clearly proved. First, application of the KPP (Kolmogorov-Petrov-Piskunov) theorem [16, 44] to a Reynolds averaged progress variable $\bar{c}$ equation (using a gradient diffusion closure and a few other assumptions on the average reaction rate [33]), can be used to show that the turbulent flame speed is controlled by the characteristics of the average reaction rate at the leading edge of the flame brush, i.e., the points where $\bar{c} \to 0$, in a statistically stationary one dimensional flame. Within this framework, the "leading point" is defined as the point where $\bar{c} \to 0$; we will refer to this point/surface as the "flame brush leading point" in this paper. Note that within this interpretation, the flame does not possess leading points for the majority of time instants, as the point on the flame that instantaneously lies farthest into the reactants may occur over a range of $\bar{c}$ values. We will refer to these points as "instantaneous leading points", indicated by the yellow "x" in Figure 1. This figure reproduces an image from Marshall *et al.* [36], where the instantaneous flame front is overlaid on top of time averaged progress variable contours. In this same paper, we analyze the curvature statistics of the point on the flame that lies farthest into the reactants: for 90% of the flame realizations this position occurs over the $0.02 < \bar{c} < 0.66$ range, with an average location at $\bar{c} \cong 0.24 - 0.30$, depending on turbulence intensity and fuel composition. Indeed, the $\bar{c} \to 0$ in any real data set of finite size lies at the point where a single realization of the flame occurs.
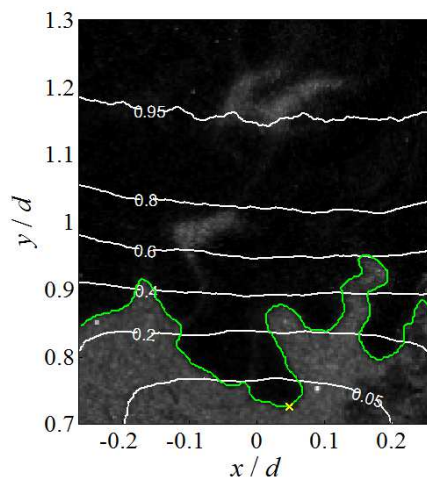
Figure 1. Mie scattering image from LSB burner of Marshall *et al.* [36] (*d* = 36*mm*, 50/50 H₂/CO, 0.55 equivalence ratio, STP conditions). Flame edge (green), instantaneous leading point (yellow x) and average progress variable, $\bar{c}$, (white) overlaid onto the raw image.

The second example that clearly shows the significance of the leading points in uniquely controlling the burning velocity is shown in Figure 2a, following Ref. [46]. This figure illustrates an initially flat flame propagating in a spatially varying, but temporally steady state, flow field in which the velocity isocontours are parallel to the direction of flame propagation. Consider the case where the laminar burning velocity, s_L, is constant, then it is seen that the portion of the flame at the highest velocity point, point "B" in the figure, propagates out the fastest. In the lab-fixed coordinate system,

the flame at Point B moves at a speed of $s_L + (\Delta u)_{LP}$, where the subscript "LP" denotes the leading point. Moreover, it can easily be shown by a front tracking computation that, after an initial transient, the entire front reaches a stationary shape and propagation speed with the value $s_L + (\Delta u)_{LP}$ as shown in Figure 2b. As such, the front displacement speed is controlled by the leading points of the flame that propagate into the highest velocity regions ahead of the flame. This example clearly illustrates that the resulting increase in flame area induced by the spatially varying velocity field is the *effect* of the higher displacement speed, not the *cause*. Finally, note that in this steady state example, the "flame brush leading point" and "instantaneous leading point" coincide.
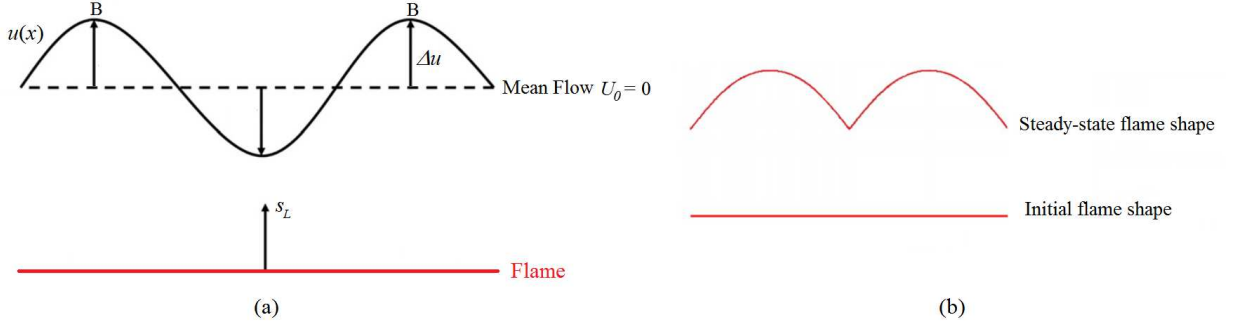
Figure 2. Model problem of a flat flame propagating into a spatially varying flow field (a); level set computation of the model problem, where the initial and final steady-state flame shapes are shown (b) [46].

More generally, if the unidirectional velocity field is given by $u(x) = f(x)$, then it can be shown by a simple geometric reasoning that the burning velocity at large times is given by $s_L + \max(f(x))$ (proved formally in Appendix B). In other words, *the burning velocity is controlled by conditions at a discrete spatial point* or points and is independent of the initial conditions and the details of the flow field, such as the scale size of the velocity inhomogeneities.

This latter model problem becomes more complicated, when the angle of flame propagation is not parallel to velocity isocontours. In this case, the spatial position of the leading point evolves in time, as a point that was propagating into the lowest velocity portion of the flow advances and moves into a higher velocity region. Following the terminology of Ref. [47, 48], the leading point may no longer be "quasi-steady", and it is unclear how to apply leading points argument in this case, or if this approach is even valid. This paper takes up this problem in detail in order to examine the dynamical significance of leading points, and to determine whether conditions exist where the propagation velocity may be controlled not by a point, but by a distribution. Specifically, this paper considers the passive (i.e. without gas expansion) propagation of a premixed flame in a one dimensional, incompressible, unsteady, periodic shear flow. In this context, it proposes a definition for points that control the displacement speed of the front, and studies their dynamics. This type of flow configuration has been previously studied as a model problem for flame propagation in inhomogeneous flow field [1, 5-7, 10, 29, 30, 45, 54], with this specific velocity field considered explicitly by Embid *et al.* [18], who presented an exact solution for the front displacement speed. This problem is re-interpreted within the leading points framework in this paper.

The paper is organized in the following manner. Section 2 describes a few results from the theory of Hamilton-Jacobi equations, which, when applied to the G-equation, lead to our proposed mathematical formulation of leading points. These ideas are then applied to a specific shear flow in Section 3, chosen because the instantaneous leading points evolve temporally, but also because is amenable to an exact solution. The laminar flame speed s_L is assumed to be constant in Sections 2 and 3. Section 4 then considers generalizations of these results to the case where the burning velocity has a linear dependence of s_L on curvature, with a positive Markstein length, ℓ. Finally, the Conclusions section considers the extension of these results to the multi-dimensional case.

2. Problem formulation and mathematical background

2.1 Problem formulation

To model the reaction front propagation, we utilize the *G-equation* [41]:

$$\frac{\partial G}{\partial t} + \vec{u}(\vec{x},t) \cdot \nabla G = s_L |\nabla G| \tag{1}$$

where the level set of the scalar function G represents the flame position, $\vec{u}(\vec{x},t)$ is the flow velocity at the flame and s_L is the (constant) laminar flame speed. Assuming a two-dimensional flame front whose location is a single valued function, ξ, of the coordinate x (see Figure 3), we define $G(x,y,t) \equiv \xi(x,t) - y$ which inserted in equation (1) leads to:

$$\frac{\partial \xi}{\partial t} + u_x(x,t)\frac{\partial \xi}{\partial x} - u_y(x,t) = s_L\sqrt{1+\left(\frac{\partial \xi}{\partial x}\right)^2} \tag{2}$$

Equation (2) is a Hamilton-Jacobi equation, whose convex Hamiltonian function is represented by $H = H(x,t,g) = -s_L\sqrt{1+g^2} + u_x g - u_y$ where $g = \partial \xi/\partial x$ is the flame slope and satisfies the conservation equation

$$\frac{\partial g}{\partial t} + \frac{\partial}{\partial x}H(x,t,g) = 0 \tag{3}$$
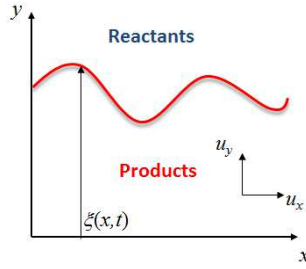
Figure 3. Schematic of a two-dimensional flame whose position is a single valued function of the x coordinate.

In this paper, we assume that u_x and u_y are periodic in (x,t) with period $[0,L] \times [0,T]$ and form an incompressible flow field. We are interested in the study of the front displacement speed at large time, s_T, defined as:

$$s_T = \frac{1}{L}\frac{1}{T}\int_0^L\int_0^T \frac{\partial \xi}{\partial t}\,dx\,dt = -\frac{1}{L}\frac{1}{T}\int_0^L\int_0^T H(x,t,g)\,dx\,dt \quad \text{for } t \to +\infty \tag{4}$$

Under the above assumptions, it can be shown that s_T exists [11], but equation (2) can admit more than one entropy solution for the same value of s_T [49]. In the context of multiscale expansions of Hamilton-Jacobi equations, s_T is also referred to as the "homogenized (or effective) Hamiltonian" (see Appendix A).

2.2 Aubry-Mather theory

In this section we present several results, proved by Weinan [49], who utilized the Aubry-Mather theory [37] to study periodic solutions of one dimensional conservation equations of the form of equation (3). Start with a few definitions. The characteristic curves associated with equation (3) satisfy the system of ordinary differential equations

$$a) \quad \frac{dx}{dt} = \frac{\partial H}{\partial g}$$
$$b) \quad \frac{dg}{dt} = -\frac{\partial H}{\partial x} \tag{5}$$

Characteristics curves describe solutions of equation (3) away from discontinuities in the graph of g which are known as "shocks" and represents cusps in the graph of ξ. Solutions of equation (2) admit also a variational representation given by

$$\xi(x,t) = \min_{\gamma \in AC, \gamma(t)=x} \left\{ \int_{\tau}^{t} L(\gamma(s), s, \dot{\gamma}(s)) ds + \xi(\gamma(\tau), \tau) \right\} \tag{6}$$

for every $\tau < t$, where AC represents the set of all Lipschitz continuous paths $\gamma : \mathbb{R} \to \mathbb{R}$ and L is the Lagrangian function (or Legendre transform) associated with the Hamiltonian H:

$$L(x,t,\dot{\gamma}) = \sup_{g}\left(g \cdot \dot{\gamma} - H(x,t,g) \right) = \sqrt{s_L^2 - (\dot{\gamma} - u_x)^2} + u_y \tag{7}$$

Equation (6) is known as the "Lax formula" [19] in the context of partial differential equation theory and the "principle of least action" [50] in the context of Hamiltonian dynamical systems theory. It can be demonstrated that the characteristic curves are solutions of the minimization problem (6) and from equation (5)a we have:

$$\dot{\gamma} = \frac{dx}{dt} = \frac{\partial H}{\partial g} \tag{8}$$

From a physical point of view, the Lagrangian represents the propagation speed in the y-direction of the point on the flame surface that follows the trajectory of the characteristic curve γ. Those curves, γ, which solve equation (6) on intervals $(-\infty, t]$ are referred to as "one-sided minimizers" and "two-sided" (or global) minimizers if they solve it on intervals $(-\infty, +\infty)$.

We now can state Weinan's results [49]:

1) For each $(x,t) \in [0,L] \times [0,T]$ at which ξ is differentiable with respect to x (i.e. away from shocks in the graph of g) there exists a unique one-sided minimizer;

2) There exist curves γ^* which solve equation (6) for any interval $[t_0, t_1]$ (i.e. γ^* is a global minimizer) and ξ is differentiable with respect to x for each $(x,t) = (\gamma^*(t), t)$; the Aubry-Mather set Γ_{AM} associated with a solution ξ of equation (2) is defined as:

$$\Gamma_{AM}(\xi) = \left\{ (\gamma(0), g(\gamma(0),0)) \; s.t. \; \gamma \text{ is a global minimizer} \right\} \tag{9}$$

3) For each one-sided minimizer γ there exists a global minimizer γ^* associated with Γ_{AM} such that $|\gamma(t) - \gamma^*(t)| \to 0$ as $t \to -\infty$.

Using result (2) and equation (6), it follows that for large times the front displacement speed (4) can be expressed as:

$$s_T = \frac{1}{T}\int_0^T L(\gamma^*(t), t, \dot{\gamma}^*(t)) dt = \frac{1}{T}\int_0^T \left(\sqrt{s_L^2 - (\dot{\gamma}^*(t) - u_x(\gamma^*(t), t))^2} + u_y(\gamma^*(t), t) \right) dt \tag{10}$$

2.3 Definition of Aubry-Mather Leading Points

To understand the physical meaning of the results presented in the previous section it is useful to visualize the Aubry-Mather set in the $x-t$ plane as the union of all global minimizers $\gamma^*(t)$. Let us return to the problem considered in the Introduction - an initially flat flame, $\xi(x,0) = g(x,0) = 0$, propagating in a steady periodic flow field,

$u_y = A\cos(2\pi x/L)$, with no transverse flow, $u_x = 0$. In this case, the characteristic curves can be obtained by solving Eq.(5) analytically [45]. Figure 4 plots the temporal evolution of g and ξ for A/s_L=0.5. It can be seen that, after an initial transient, the solution develops a shock in the graph of g (a cusp the graph of ξ) at $x/L = 0.5$, which grows until the steady state is reached. The characteristics curves of these solutions are plotted in the $x-t$ plane in Figure 5. Note that the only trajectories that are never absorbed by the shock correspond to the positions where u_y is maximum. These trajectories, according to result (2) in the previous paragraph, represent the global minimizers and, from Eq. (10), the front displacement speed can be readily obtained as

$$s_T = A + s_L \tag{11}$$

The *characteristic curve trajectories that belong to the Aubry-Mather set uniquely determine the large-time behavior of the flame propagation*. In contrast, the dynamics of the one-sided minimizers, which form the "domain of attraction" of the shock [25], determines the overall shape of the flame (as it will become clearer in next paragraph), but do not provide any information about the large-time front displacement speed.
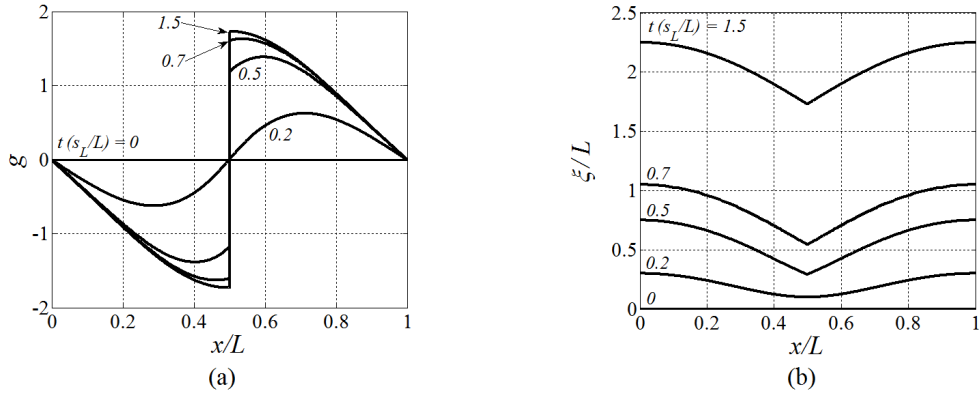

(a)   (b)

Figure 4. Flame slope g (a) and flame shape ξ (b) at different normalized times $t(s_L/L)$ for the flow field

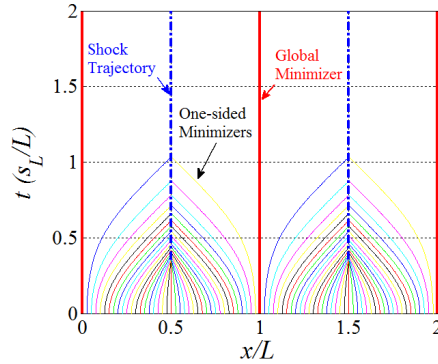$$u_y = A\cos(2\pi x/L),\ u_x = 0\ \text{with}\ A/s_L = 0.5.$$

Figure 5. Characteristics curves in the x - t plane for the solutions showed in Figure 4. One-sided minimizers are represented by variously colored thin lines, global minimizers by thick red lines and the shocks trajectories by thick blue dot-dashed lines.

We define "Aubry-Mather points" as those parts of the flame that belong to the Aubry-Mather set, i.e. whose propagation follows the trajectories of the global minimizers. *However, in general, the global minimizers may not be isolated trajectories and, as such, they may not be discrete points on the flame* as the name "leading points" seems to suggest. For instance, if in the example above we had chosen a function with degenerate (i.e. with zero second derivative) absolute maxima to represent the steady shear flow profile, then the trajectories of the global minimizers could originate from a continuous band of spatial positions. This is one of the reasons why, in result (2) cited in the previous section, uniqueness of global minimizers in each spatial period is not guaranteed. In the context of the

6

Hamiltonian dynamical system defined by equations (5), when the trajectories of the global minimizers are isolated from each other, they are also known as "hyperbolic trajectories" [50]. When the system is autonomous (i.e., without explicit time dependence, as for the example of Figure 4 and Figure 5) they may be also referred to as "hyperbolic fixed (or equilibrium) points", since they are equilibrium points for the characteristics in Eq. (5). In the case of a flame propagating in a unidirectional steady shear flow ($u_y = f(x)$, $u_x = 0$), it can be shown that the Aubry-Mather points are hyperbolic points (i.e. a finite number of isolated points) only if $f(x)$ possesses a finite number of non-degenerate absolute maxima for $x \in [0, L]$ [35]. Thus, this analysis suggests a third potential leading point definition, which we refer to as the "Aubry-Mather Leading points", as those parts of the flame that belong to the Aubry-Mather set, in the case where these points belongs to hyperbolic trajectories.

3. Model problem

In this section we consider a flame propagating in a periodic steady shear flow $u_y = f(x)$ with a constant mean transverse wind $u_x = V \geq 0$. Equation (2) admits an analytical solution [18] for this flow field, which is reproduced in the Appendix A. With a change in coordinate system, this problem is also equivalent to a flame propagating at an angle of $\alpha = \tan^{-1}(V/s_T)$ to the velocity isocountours of u_y. In this framework, the mean transverse wind V can be interpreted as a parameter of the "unsteadiness" of the axial flow u_y since in a reference frame attached to the transverse flow (moving in the x-direction with velocity V) the Galilean transformations

$$
\begin{aligned}
x' &= x + Vt & u_x' &= u_x - V = 0 \\
t' &= t & u_y' &= u_y
\end{aligned}
\tag{12}
$$

eliminate the transverse mean flow, with the shear flow now being time dependent $u_y'(x,t) = f(x' - Vt')$. In this new reference frame, the shear is therefore acting on the flame with a time-scale given by L/V, where L is the spatial period of $u_y(x)$. The competition between this time scale and the time scale associated with flame propagation, which can be taken as proportional to L/s_L, generates rich and interesting behavior [10]. In fact, the rate at which the front displacement speed s_T is enhanced by increasing flow intensity A is reduced as the unsteadiness V grows, analogous to one of the mechanism leading to the "bending effect" discussed in the turbulent combustion literature [7].

In order to develop our examples, we consider two periodic flow fields: one consisting of a single harmonic

$$
u_y(x) = A \cos(2\pi x/L)
\tag{13}
$$

and one with multiple harmonics

$$
u_y(x) = \frac{2}{5}A\cos(2\pi x/L) + \frac{A}{5}\sin(2\pi x/L) + \frac{A}{5}\cos(4\pi x/L) + \frac{A}{5}\cos(6\pi x/L) - \frac{A}{10}\sin(6\pi x/L) + \frac{A}{5}\cos(8\pi x/L)
\tag{14}
$$

The shear flow (14) was considered also in references [17, 18] as an example of a profile with a complex structure and an asymmetrical form with multiple local maxima and minima. Figure 6a shows the dependence of s_T on the shear flow amplitude A for both profile (13) and (14) at different value of "unsteadiness parameter", V. Its inhibiting effect is illustrated by the fact that when no unsteadiness is present ($V = 0$) s_T depends linearly on A, and is given by equation (11) for both shear flow profiles, while the front displacement speed monotonically decreases for increasing V. Figure 6b replots these same data in terms of normalized enhancement of the displacement speed $(s_T - s_L)/A$ in order to better illustrate this effect. Here, the significance of increasing V on decreasing the displacement speed is clearly shown. At large enough values of V, s_T always asymptotes to s_L. However, s_T exceeds s_L for a larger range of V values with increasing amplitude, A.
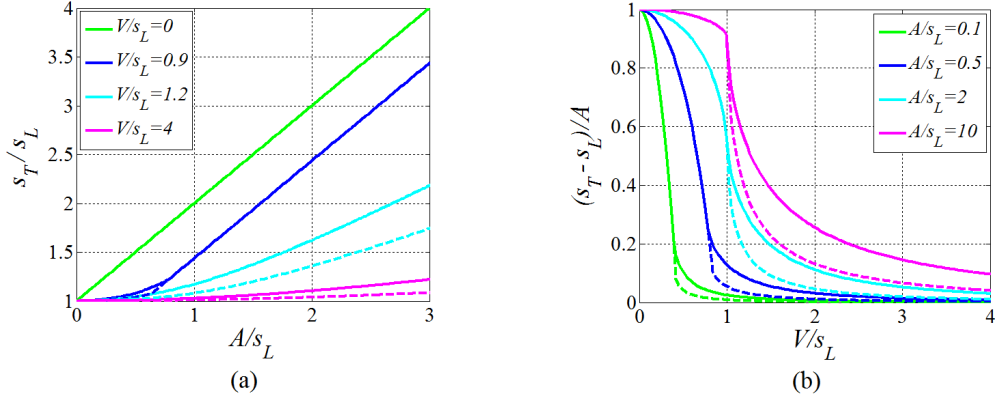
Figure 6. Dependence of front displacement speed s_T on shear flow amplitude A for fixed unsteadiness parameter V (a). Normalized enhancement of displacement speed $(s_T - s_L)/A$ as a function of unsteadiness parameter V at fixed shear flow amplitude A (b). Solid lines refer to the shear flow profile (13) while dashed lines refer to the shear flow profile (14).

The classical interpretation of these effects is in terms of flame area. To illustrate, Figure 7 plots flame shapes at the steady state for a fixed shear flow amplitude ($A/s_L = 0.5$) and different values of transverse wind intensity. It can be observed how the overall flame area decreases as the unsteadiness parameter V increases. However, this explanation does not clarify why, for certain values of A and V, the front displacement speed is identical for the two shear flow configurations, while it is different for other combination of A and V. Specifically, Figure 6, shows that s_T values are different for the two shear flow profiles (i.e. dashed and solid lines are not superimposed) for large values of unsteadiness V.
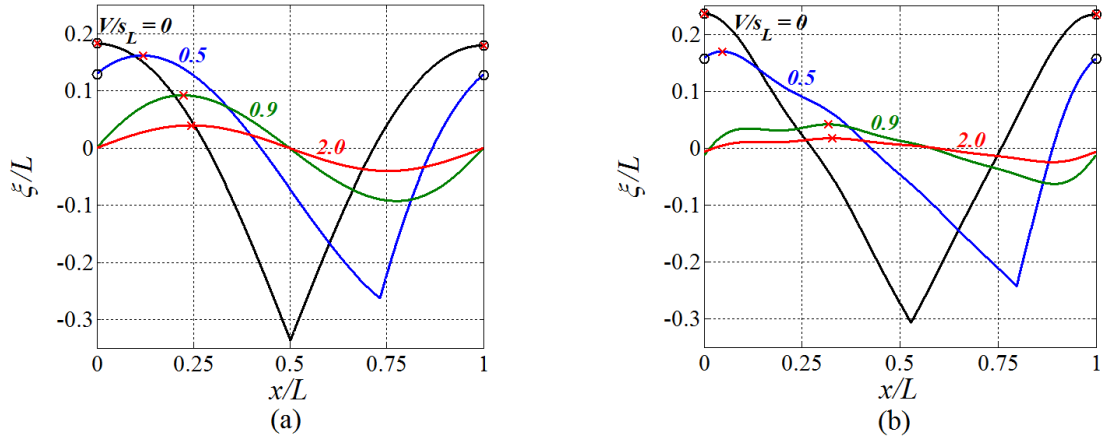

Figure 7. Flame shape ξ for $A/s_L = 0.5$ and different values of V/s_L for both profile (13) (a) and profile (14) (b). The graphs of ξ are adjusted so that their average is zero. "Aubry-Mather leading points" are indicated by black circles (which only exist for the $V/s_L = 0$ and 0.5 cases); "instantaneous leading points" are indicated by red crosses.

We now show that the differences in the occurrence of the inhibiting effect between shear flow profile (13) and (14) can be interpreted in terms of the dynamics of global minimizers (i.e. in terms of the "Aubry-Mather leading points"). First we remark that both profiles (13) and (14) have only one absolute maxima per period, occurring at $x = kL$ $(k \in \mathbb{N})$, where $u_y(kL) = A$. According to the discussion in the previous section then, for $V = 0$ the solution of equation (2) possess a unique hyperbolic global minimizer per period whose position coincides with the absolute maxima in velocity. A convenient way to visualize the global minimizers in the $x - t$ plane is to solve the characteristics equations (5) backward in time since, as stated in result 2) in the previous section, all the characteristics curves (one-sided minimizers) converge to the global minimizers for $t \to -\infty$ [40]. Figure 8 and Figure 9 illustrate these backward characteristic curves for the solutions plotted in Figure 7. Figure 8a and Figure 9a show that when no unsteadiness in the

8

flow is present ($V/s_L = 0$) the global minimizers at $x = kL$ ($k \in \mathbb{N}$) are hyperbolic fixed points for both shear flow profiles. Then, from equation (10), it is clear that both profiles yield the same front displacement speed since $u_y(kL) = A$. This conclusion is not influenced by the trajectories of the one-sided minimizers which determine the details of the flame shape and depend on the form of the shear flow profile u_y. From Figure 8b and Figure 9b, it is clear that a limited amount of "unsteadiness" in the flow does not alter the trajectory and the hyperbolic character of the global minimizers. In this case, the front displacement speed and its observed bending with increasing V are the same for both shear flows. Examining the flame shapes plotted in Figure 7 for $V/s_L = 0.5$, it also interesting to notice that the discrete global minimizer trajectory does not correspond to the most forward-lying position of the flame – *i.e., the "Aubry-Mather leading points" and the "instantaneous leading points" do not coincide*. In other words, the points controlling the front displacement speed are not the most forward-lying position of the flame front in the direction of the reactants.

A bifurcation in solution characteristics occurs when the unsteadiness parameter, V, reaches a critical value. For example, in Figure 8c and Figure 9c *all* the trajectories are global minimizer and their hyperbolic character is lost. In this case, the trajectories of the global minimizers depend on the spatial details of the shear flow structure, and the two profiles (13) and (14) yield different values of front displacement speed according to equation (10).

(a)   (b)   (c)
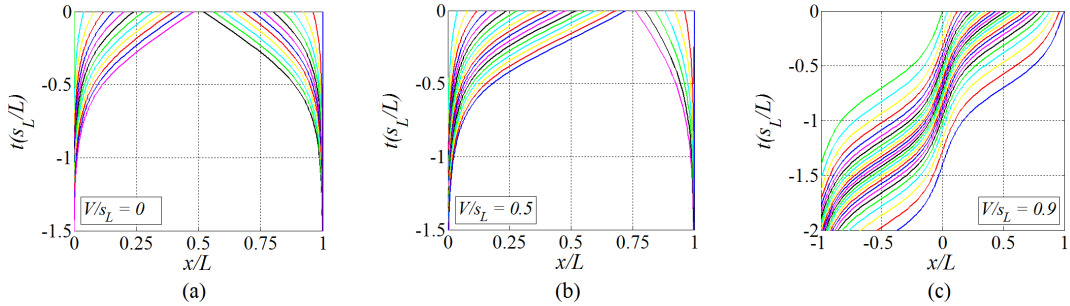
Figure 8. Backward characteristic curves in the x-t plane corresponding to the solutions shown in Figure 7a (shear flow profile of equation (13) with $A/s_L = 0.5$).

(a)   (b)   (c)
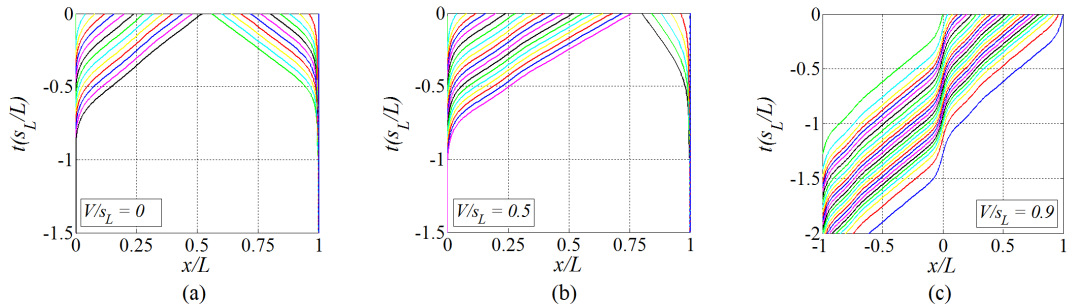
Figure 9. Backward characteristic curves in the x-t plane corresponding to the solutions shown in Figure 7b (shear flow profile of equation (14) with $A/s_L = 0.5$).

From the analytical solution, it is possible to solve for the parameter values A and V where the hyperbolic fixed point is lost, as plotted in Figure 10. The figure shows that for $V > s_L$ the unsteadiness is too high and no fixed points are presents for all values of A. At low A values, the fixed point can be lost even at lower values of V. This situation mirrors the trends shown in Figure 6.
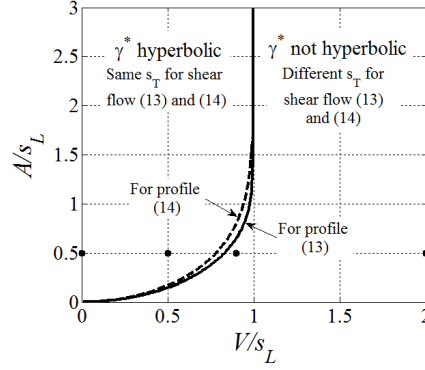
Figure 10. Parameter space A - V divided into regions in which solutions of the model problem admit and do not admit hyperbolic global minimizers. Dots indicate the conditions at which solutions plotted in Figure 7 are obtained.

Two key results emerge from this section. First, under certain conditions, the front displacement speed is controlled by velocity field characteristics at discrete points on the flame, points we define as "Aubry-Mather leading points". However, these points do not generally lie on the farthest forward point of the front (the "instantaneous leading point"). Under these conditions, two totally different velocity fields with the same maximum value lead to identical front displacement speeds. Second, for other conditions, the front displacement speed is not controlled by discrete points, but rather by the entire spatial distribution of the velocity field. For these conditions, the "instantaneous leading points" do not have any dynamical significance in controlling the front displacement speed. The extent to which these two results modify proposed leading point arguments as articulated in the Introduction remains to be seen, however, as care must be exercised in translating results from this deterministic problem to the ensemble average characteristics of a stochastic problem that is of interest to determining the front displacement speed.

4.   Curvature effects

The previous section considered the case where the laminar burning velocity was constant. In reality, it is well known that the laminar burning velocity is a function of the flame stretch rate for reactants with non-zero Markstein lengths that, in turn, is a function of the local flow shear and flame curvature. For example, several DNS studies of turbulent premixed flames have shown that local changes of flame speed correlate strongly with the local curvature of the flame front [34, 43]. In this section, we incorporate a curvature sensitivity into the burning velocity, by means of the following expression, valid for weak stretch:

$$s_L = s_{L,0}\left(1 - \ell\kappa\right) = s_{L,0}\left(1 + \ell\,\frac{\partial^2\xi/\partial x^2}{\left(1 + \left(\partial\xi/\partial x\right)^2\right)^{3/2}}\right) \tag{15}$$

where $s_{L,0}$ represents the laminar unstretched flame speed, ℓ is the Markstein length and κ represents the curvature. For weak curvature (i.e., where the amplitude of wrinkling is small relative to the transverse length scale of wrinkling), this expression can be further linearized and, when inserted into the G-equation, yields an additional "viscous" term [28]:

$$\frac{\partial\xi}{\partial t} + u_x\frac{\partial\xi}{\partial x} - u_y = s_{L,0}\sqrt{1 + \left(\frac{\partial\xi}{\partial x}\right)^2} + s_{L,0}\ell\frac{\partial^2\xi}{\partial x^2} \tag{16}$$

In this section, we consider the evolution of equation (16) for $\ell > 0$ (i.e. a positive Markstein length, a thermo-diffusionally stable flame). The negative Markstein length case is a subject of ongoing investigation. Equation (16) admits a variational solution, similar to equation (7), but with a small white noise added [8, 21]:

$$\xi(x,t) = \min_Y E\left\{\int_\tau^t L\big(r(s),\dot{\eta}(s),s\big)ds + \xi\big(r(\tau),\tau\big)\right\} \tag{17}$$

where r solves for $\tau < s \leq t$ the stochastic differential equation

$$\begin{cases} dr(s) = Y\big(r(s),s\big)ds + \sqrt{2s_{L,0}\ell}\, dw(s) \\ r(t) = x \end{cases} \tag{18}$$

and Y varies in the class of smooth, time dependent functions, $\dot{\eta}(s) = Y\big(r(s),s\big)$, w represents the one dimensional Wiener process and E denotes the expectation with respect to the Wiener measure. If we call Y_ℓ the minimal Y in equation (17) (which exists and is unique [21]) and r_ℓ the solution of the corresponding stochastic differential equation (18) then it is possible to obtain a formula analogous to equation (8) [21]

$$\dot{\eta}_\ell(s) = Y_\ell(x,s) = \frac{\partial}{\partial g}H(x,s,g) \tag{19}$$

Despite being presented here for the one dimensional case, we remark that the stochastic variational representation can be extended to the three dimensional viscous G-equation, as described in Ref. [20]. Based on formula (17), it is also possible to extend the Aubry-Mather theory presented in Section 2.2 [22]. From a physical point of view, the effect of the viscous term can be interpreted as a diffusion that "blurs" the otherwise "sharp" trajectory of the global minimizer. It seems intuitive to expect that the strength of this effect depends on the behavior of $\partial^2\xi/\partial x^2$ along the global minimizers trajectories (i.e. of the "curvature" at the leading points). If the Aubry-Mather set for the inviscid problem consists of finite number of hyperbolic trajectories in each period, then it can be shown that this intuitive physical picture is indeed correct. Let us define the large-time average value of $\partial^2\xi/\partial x^2$ following the i-th global minimizer for the inviscid problem as

$$C_i \equiv \frac{1}{T}\int_0^T \frac{\partial^2}{\partial x^2}\xi\big(\gamma_i^*(s),s\big)ds \qquad t \to +\infty \tag{20}$$

and assume that, among all the global minimizers, there exist only one $C_I = \min_i C_i$ per period. Then, it can be demonstrated that [4, 8]

$$\frac{1}{s_{L,0}}\lim_{\ell \to 0}\frac{\partial s_T}{\partial \ell} = C_I \tag{21}$$

To illustrate, we consider the effect of the viscous term for the model problem described in Section 3 for shear flow (13) and (14) in the $A-V$ parameter space where the solution possesses a unique, hyperbolic global minimizer per period (see Figure 10). Using the analytical solution in equation (31), the value of C_I for both profiles are given by:

$$C_I = -\frac{s_{L,0}}{\left(s_{L,0}^2 - V^2\right)^{3/4}}\sqrt{-\frac{\partial^2 u_y}{\partial x^2}(x=0)} = \begin{cases} -\dfrac{2\pi}{L}\dfrac{s_{L,0}\sqrt{A}}{\left(s_{L,0}^2 - V^2\right)^{3/4}} & \text{for shear flow (13)} \\[4mm] -\dfrac{\sqrt{155}}{5}\dfrac{2\pi}{L}\dfrac{s_{L,0}\sqrt{A}}{\left(s_{L,0}^2 - V^2\right)^{3/4}} & \text{for shear flow (14)} \end{cases} \tag{22}$$

This expression clearly shows the inhibiting effect that a positive Markstein length has on the front displacement speed. This result is well known from measurements of turbulent flame speeds of lean, heavy fuels [15, 34].

The effect of the curvature term is stronger for the shear flow (14), since the absolute maxima at $x = 0$ is sharper. To analyze equation (21)-(22), equation (16) was solved numerically to extract the value of s_T. The computational scheme discretized first order spatial derivatives in equation (16) using a fifth-order WENO scheme [26] and a central sixth-order scheme for the second order spatial derivative. A Total Variation Diminishing (TVD), third order Runge–Kutta scheme [23] was used for time integration and the Local Lax-Friedrich (LLF) scheme was used for improved stability [26]. The comparison between the numerical computation of s_T and the linear relation (21) for different values of A and V is shown in Figure 11. These results show that equation (21)-(22) exactly captures the dependence of s_T upon ℓ for $\ell/L \ll 1$, especially when the value of $\partial^2 \xi / \partial x^2$ at the leading point is not too high (such as for shear flow (13) in Figure 11a). For high values of $\partial^2 \xi / \partial x^2$, the dependence of s_T on ℓ becomes nonlinear, and the linearized approximation loses accuracy.
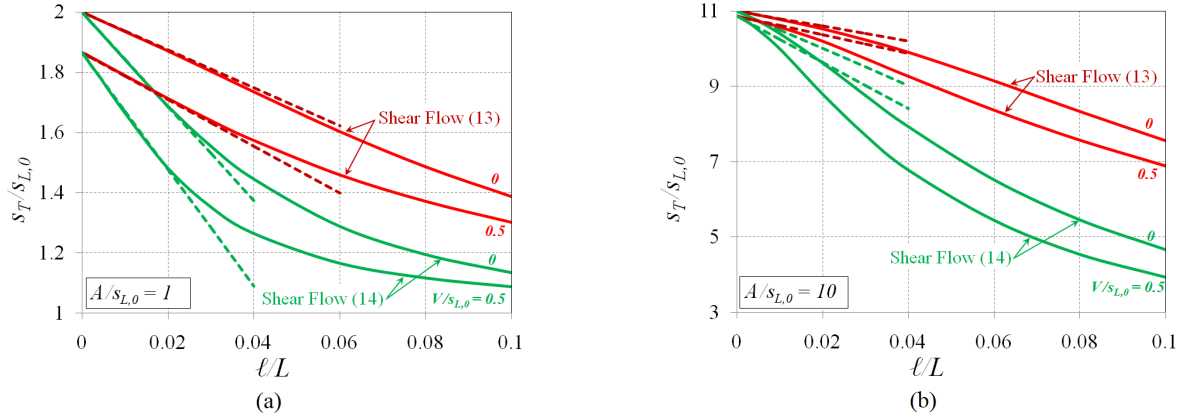
Figure 11. Front displacement speed s_T dependence on Markstein length ℓ for $A/s_L = 1$ (a), $A/s_L = 10$ (b) and different V values for the model problem of Section 3. Solid lines refer to numerical solutions, dashed lines to the linear approximation of equation (21).

5. Concluding Remarks

In order to assess phenomenological leading points arguments, this paper has analyzed exact solutions for flame propagation in periodic shear flows. These results validate some basic ideas from Zeldovich's leading points arguments, but also modify them appreciably, at least for this deterministic problem. In particular, these results clearly show that under certain conditions, the front displacement speed is controlled by velocity field characteristics at discrete points on the flame. However, these points do not generally lie on the farthest forward point of the front (the "instantaneous leading point"). Second, for other conditions, the front displacement speed is not controlled by discrete points, but rather by the entire spatial distribution of the velocity field. For these conditions, the "instantaneous leading points" do not have any dynamical significance in controlling the front displacement speed. Finally, these results clearly show the effects of flame's stretch sensitivity in modifying the front displacement speed can be successfully interpreted in term of leading point concepts.

A natural question at this point is if the ideas applied in the previous sections apply to the G-equation (1) in two and three dimensional flows where the flame position is not a single valued function of x. Unfortunately, the existence of global minimizers is not guaranteed in general, and the ideas described in the previous sections need to be applied with care. To illustrate why this is the case, let us start recalling that for an autonomous Hamilton-Jacobi equation

$$\frac{\partial \varphi}{\partial t} + H\left(\vec{x}, \nabla \varphi\right) = 0 \quad \vec{x} \in \Omega \subset \mathbb{R}^n \tag{23}$$

12

(with the Hamiltonian function H convex in the $\nabla\varphi$ variable), a sufficient condition for the existence of the Aubry-Mather set is for the Hamiltonian to satisfy the so called coercivity condition[1] [24]:

$$\lim_{|\nabla\varphi|\to+\infty} H(\vec{x},\nabla\varphi) = +\infty \tag{24}$$

For the G-equation, the Hamiltonian $H(x,\nabla G) = s_L|\nabla G| - \vec{u}(x)\cdot\nabla G$, does not satisfy Eq. (24) for a mean-zero velocity field $\vec{u}(x)$ with amplitude larger than then the laminar flame speed s_L. From a physical point of view the lack of coercivity means that the propagation of the flame front is dominated by stirring and convection, rather than actual flame propagation, and it is possible that certain flow profiles can "block" characteristic curves and prevent them from existing on time intervals $(-\infty,+\infty)$ (i.e. prevent it from being a global minimizer) [52]. For flow fields that do not admit an Aubry-Mather set, some success in studying front displacement speeds trends has been made considering "local action minimizing trajectories" [42, 53], which seem to bear an analogy to the global minimizers but in a local setting. Also, locally minimizing trajectories have been used to demonstrate mathematically the existence of the front displacement speed in periodic and random incompressible flows in any dimension [12]. However, at this point is not clear if the dynamics of these local trajectories is analogous to the dynamics of global minimizers as presented in this paper. Extension of the present model to more complex flow configurations will be the subject of future works.

Appendix A

In this Appendix we describe the analytical solution of model problem of Section 3 [18]. This solution is obtained through an averaging procedure (homogenization) for the G-equation applicable when the velocity flow field in which the flame is moving is composed by spatially and temporally separated scales. Let us assume that $\vec{u}$ in equation (1) is an incompressible velocity field with two separated spatial scales $\vec{u} = \vec{\bar{v}}(\vec{x}) + \vec{v}(\vec{x}/\varepsilon)$, where ε is a small parameter representing the ratio of the two length scales of the velocity field: in this context it is natural to seek a solution G in the form of an asymptotic multiscale expansion

$$G = G^0(\vec{x},t) + \varepsilon G^1(\vec{x},\vec{x}/\varepsilon,t) + \dots \tag{25}$$

Substituting Eq. (25) into Eq.(1) at the leading order we obtain

$$\frac{\partial G^0}{\partial t} + \left(\vec{\bar{v}}(\vec{x}) + \vec{v}(\vec{y})\right)\cdot\left(\nabla_{\vec{x}}G^0 + \nabla_{\vec{y}}G^1\right) - s_L\left|\nabla_{\vec{x}}G^0 + \nabla_{\vec{y}}G^1\right| = 0 \tag{26}$$

where $\vec{y} = \vec{x}/\varepsilon$. The objective of the homogenization procedure is to describe the motion of the larger scale G^0 in terms of the smaller scale G^1, namely, to obtain the effective propagation speed $s_T(\vec{P},\vec{x})$ of the large scale for a given position $\vec{x}$ and direction of propagation $\vec{P} = -\nabla_{\vec{x}}G^0$:

$$\frac{\partial G^0}{\partial t} = s_T(\vec{P},\vec{x}) \tag{27}$$

where

$$s_T(\vec{P},\vec{x}) = -\left(\vec{\bar{v}}(\vec{x}) + \vec{v}(\vec{y})\right)\cdot\left(-\vec{P} + \nabla_{\vec{y}}G^1\right) + s_L\left|-\vec{P} + \nabla_{\vec{y}}G^1\right| \tag{28}$$

---

[1]Note that for the one-dimensional problem considered in Section 3, the global minimizer does exist even though the problem does not satisfy the coercivity condition for $V \geq s_L$.

Equation (28) is a nonlinear eigenvalue problem, referred to as the flame "cell problem" [51]. If the larger scale is a constant $\vec{\bar{v}}(\vec{x}) = const$ (i.e. its period is infinite) the ansatz (25) is an exact solution, and the discussion on the multiscale expansion has only a motivational purpose. In our model problem, we considered a two scale flow with $\vec{\bar{v}}(\vec{x}) = (V,0) = const$ and $\vec{v}(\vec{x}/\varepsilon) = (0, f(x))$, where $f(x)$ is periodic of period L and zero mean; our choice of $G = \xi(x,t) - y$ in equation (2) is equivalent to imposing $G^0 = -y$ and $G^1 = \xi(x,t)$ with the mean direction of propagation now being $\vec{P} = (0,1)$. With these choices equation (28) reduces to:

$$s_T = s_L \sqrt{1 + g^2} - Vg + f(x) \tag{29}$$

The eigenfunction g of this nonlinear eigenvalue problem has to satisfy a periodicity condition

$$\frac{1}{L}\int_0^L g\, dx = \bar{g} = 0 \tag{30}$$

This average slope $\bar{g}$ can also be interpreted as a conserved quantity for the conservation equation (3), since its dynamics does not modify $\bar{g}$. For Hamiltonians of the mechanical type, $H(x,t,p) = p^2/2 + f(x,t)$, this quantity represents an average momentum of the system [49]. Equations (29)-(30) can be solved using the procedure presented in Table 1. This is a simplified version of the procedure in Ref. [18] which include a general dependence on mean direction of propagation $\vec{P} = (\cos\theta, \sin\theta)$ and the constant large scale velocity $\vec{\bar{v}}(\vec{x}) = V(\cos\bar{\theta}, \sin\bar{\theta}) = const$.

Define $s_T^* = \sqrt{s_L^2 - V^2} + \max(f(x))$ and the function $F^{-1}(z) = \dfrac{-Vz + s_L\sqrt{z^2 + (V^2 - s_L^2)}}{V^2 - s_L^2}$:

1. If $V > s_L$ then s_T solves the nonlinear algebraic equation
$$\int_0^L F^{-1}(s_T - f(x))dx = 0$$

2. If $V < s_L$

    a. if $\int_0^L F^{-1}(s_T^* - f(x))dx < 0$ then $s_T = s_T^*$;

    b. else s_T solves the same nonlinear algebraic equation as in case 1.

3. If $V = s_L$ the solution yields a point where $g = +\infty$ (i.e. a point where the flame is parallel to the y-axis) and is not well described by equation (2). The solution of this case can be obtained as a limit from above of case 1 or from below of case 2

Table 1. Procedure used to calculate the front displacement speed, s_T, for the model problem considered in Section 3.

Once s_T has been calculated, the flame shape can be calculated solving equation (29) for g :

$$g_\pm = \frac{V(s_T - f(x)) \pm s_L\sqrt{V^2 - s_L^2 + (s_T - f(x))^2}}{s_L^2 - V^2} \tag{31}$$

Equation (31) has two branches. For case 1 and case 2b in Table 1 the only physical solution is g_-, since it is the only one that satisfies the periodicity condition (30). For case 2a in Table 1, the physical solution g jumps between the two branches. These jumps are at points where $f(x)$ reaches an absolute maximum ("transition points") and at points where g is discontinuous ("shocks"). The only rules that regulate these jumps are the entropy condition $g(x_0^+) - g(x_0^-) > 0$ across a shock at x_0 and the respect of the periodicity condition (30).

Appendix B

In this Appendix we show how the large time front speed s_T for a flame propagating in a unidirectional periodic velocity field $u_y(x) = f(x)$, $u_x = 0$ can be obtained through a simple geometric reasoning, as mentioned in the Introduction. For the flow field under consideration equation (29) becomes:

$$s_T = s_L \sqrt{1 + g^2} + f(x) \tag{32}$$

When the flame front has reached a steady state, at points where $f(x)$ has an absolute maximum the flame slope g is zero, by geometric necessity. Then, equation (32) can be readily solved, obtaining

$$s_T = s_L + \max\left(f(x)\right) \tag{33}$$

This result is independent of the particular details of the shear flow profile $f(x)$ and is a particular solution of case 2a in Table 1.

References

1. Aldredge, R.C., *The propagation of wrinkled premixed flames in spatially periodic shear flow.* Combustion and Flame, 1992. **90**(2): p. 121-133.
2. Aluri, N.K., S. Reddy Muppala, and F. Dinkelacker, *Substantiating a fractal-based algebraic reaction closure of premixed turbulent combustion for high pressure and the Lewis number effects.* Combustion and Flame, 2006. **145**(4): p. 663-674.
3. Amato, A., M. Day, R. Cheng, J. Bell, and T. Lieuwen, *Leading Point Statistics of a Turbulent, Lean, H_2-Air Flame*, in *Spring Technical Meeting of the Central States Section of the Combustion Institute* 2012: Dayton, Ohio, USA.
4. Anantharaman, N., R. Iturriaga, P. Padilla, H. Sánchez-Morgado, J. Banasiak, M. Mokhtar-Kharroubi, N. Carlsson, G. Högnäs, J. Chazottes, and E. Ugalde, *Physical solutions of the Hamilton-Jacobi equation.* Discrete and Continuous Dynamical Systems-Series B, 2005. **5**(3).
5. Ashurst, W.T., G.I. Sivashinsky, and V. Yakhot, *Flame front propagation in nonsteady hydrodynamic fields.* Combustion Science and Technology, 1988. **62**(4): p. 273-284.
6. Ashurst, W.T. and G.I. Sivashinsky, *SHORT COMMUNICATION On Flame Propagation Through Periodic Flow Fields.* Combustion Science and Technology, 1991. **80**(1): p. 159-164.
7. Ashurst, W.T., *Flow-frequency effect upon Huygens front propagation.* Combustion Theory and Modelling, 2000. **4**(2): p. 99-105.
8. Bessi, U., *Aubry-mather theory and Hamilton-Jacobi equations.* Communications in mathematical physics, 2003. **235**(3): p. 495-511.
9. Bilger, R.W., S.B. Pope, K.N.C. Bray, and J.F. Driscoll, *Paradigms in turbulent combustion research.* Proceedings of the Combustion Institute, 2005. **30**(1): p. 21-42.
10. Bourlioux, A., *Semi-analytical validation of a dynamic large-eddy simulation procedure for turbulent premixed flames via the G-equation.* Combustion Theory and Modelling, 2000. **4**(4): p. 363-389.
11. Cardaliaguet, P., J. Nolen, and P.E. Souganidis, *Homogenization and Enhancement for the G-Equation.* Archive for Rational Mechanics and Analysis, 2011. **199**(2): p. 527-561.
12. Cardaliaguet, P. and P.E. Souganidis, *Homogenization and enhancement of the G-equation in random environments.* arXiv preprint arXiv:1110.1760, 2011.

13. Damköhler, G., *Der einfluß der turbulenz auf die flammengeschwindigkeit in gasgemischen.* Zeitschrift für Elektrochemie und angewandte physikalische Chemie, 1940. **46**(11): p. 601-626.

14. Dinkelacker, F., B. Manickam, and S. Muppala, *Modelling and simulation of lean premixed turbulent methane/hydrogen/air flames with an effective Lewis number approach.* Combustion and Flame, 2011. **158**(9): p. 1742-1749.

15. Driscoll, J.F., *Turbulent premixed combustion: Flamelet structure and its effect on turbulent burning velocities.* Progress in Energy and Combustion Science, 2008. **34**(1): p. 91-134.

16. Duclos, J., D. Veynante, and T. Poinsot, *A comparison of flamelet models for premixed turbulent combustion.* Combustion and Flame, 1993. **95**(1-2): p. 101-117.

17. Embid, P.F., A.J. Majda, and P.E. Souganidis, *Effective geometric front dynamics for premixed turbulent combustion with separated velocity scales.* Combustion Science and Technology, 1994. **103**(1): p. 85-115.

18. Embid, P.F., A.J. Majda, and P.E. Souganidis, *Comparison of turbulent flame speeds from complete averaging and the G-equation.* Physics of Fluids, 1995. **7**(8): p. 2052-2060.

19. Evans, L.C., *Partial differential equations. Graduate studies in mathematics 19.* American Mathematical Society, 1998.

20. Fedotov, S., *G-equation, stochastic control theory and relativistic mechanics of a particle moving in a random field.* Combustion Theory and Modelling, 1997. **1**(1): p. 1-6.

21. Fleming, W.H., *The Cauchy problem for a nonlinear first order partial differential equation.* J. Differential Equations, 1969. **5**: p. 515-530.

22. Gomes, D.A., *A stochastic analogue of Aubry-Mather theory.* Nonlinearity, 2002. **15**(3): p. 581-603.

23. Gottlieb, S. and C.W. Shu, *Total variation diminishing Runge-Kutta schemes.* Math. Comput., 1998. **67**(221): p. 73-85.

24. Ishii, H. *Asymptotic solutions for large time of Hamilton Jacobi equations.* in *Proceedings oh the International Congress of Mathematicians: Madrid, August 22-30, 2006: invited lectures.* 2006.

25. Jauslin, H.R., H.O. Kreiss, and J. Moser. *On the forced Burgers equation with periodic boundary conditions.* in *Proceedings of symposia in pure Mathematics.* 1999. American Mathematical Society.

26. Jiang, G.S. and D. Peng, *Weighted ENO Schemes for Hamilton-Jacobi Equations.* SIAM Journal on Scientific computing, 2000. **21**(6): p. 2126-2143.

27. Karpov, V., A. Lipatnikov, and V. Zimont, *A test of an engineering model of premixed turbulent combustion.* Symposium (International) on Combustion, 1996. **26**(1): p. 249-257.

28. Kerstein, A.R. and W.T. Ashurst, *Passage rates of propagating interfaces in randomly advected media and heterogeneous media.* Physical Review E, 1994. **50**(2): p. 1100.

29. Khouider, B., A. Bourlioux, and A.J. Majda, *Parametrizing the burning speed enhancement by small-scale periodic flows: I. Unsteady shears, flame residence time and bending.* Combustion Theory and Modelling, 2001. **5**(3): p. 295-318.

30. Kortsarts, Y., L. Kagan, and G. Sivashinsky, *Flame extinction by spatially periodic shear flows.* Combustion Theory and Modelling, 2002. **6**(2): p. 189-195.

31. Kuznetsov, V.R. and V.A. Sabel'nikov, *Turbulence and combustion.* 1990, New York: Hemisphere Publishing.

32. Lipatnikov, A. and J. Chomiak, *Lewis number effects in premixed turbulent combustion and highly perturbed laminar flames.* Combustion Science and Technology, 1998. **137**(1-6): p. 277-298.

33. Lipatnikov, A. and J. Chomiak, *Turbulent flame speed and thickness: phenomenology, evaluation, and application in multi-dimensional simulations.* Progress in Energy and Combustion Science, 2002. **28**(1): p. 1-74.

34. Lipatnikov, A. and J. Chomiak, *Molecular transport effects on turbulent flame propagation and structure.* Progress in Energy and Combustion Science, 2005. **31**(1): p. 1-73.

35. Liu, Y.Y., J. Xin, and Y. Yu, *Asymptotics for turbulent flame speeds of the viscous G-equation enhanced by cellular and shear flows.* Archive for Rational Mechanics and Analysis, 2011. **202**(2): p. 461-492.

36. Marshall, A., P. Venkateswaran, J. Seitzman, and T. Lieuwen, *Measurements of leading point conditioned statistics of high hydrogen content fuels*, in *8th U. S. National Combustion Meeting* 2013: Park City, UT.

37. Moser, J., *Recent developments in the theory of Hamiltonian systems.* SIAM review, 1986. **28**(4): p. 459-485.

38. Muppala, S., N.K. Aluri, F. Dinkelacker, and A. Leipertz, *Development of an algebraic reaction rate closure for the numerical calculation of turbulent premixed methane, ethylene, and propane/air flames for pressures up to 1.0 MPa.* Combustion and Flame, 2005. **140**(4): p. 257-266.

39. Muppala, S., M. Nakahara, N. Aluri, H. Kido, J. Wen, and M. Papalexandris, *Experimental and analytical investigation of the turbulent burning velocity of two-component fuel mixtures of hydrogen, methane and propane.* International Journal of Hydrogen Energy, 2009. **34**(22): p. 9258-9265.

40. Nishida, T. and K. Soga, *Difference approximation to Aubry-Mather sets of the forced Burgers equation.* Nonlinearity, 2012. **25**(9): p. 2401-2422.
41. Peters, N., *Turbulent combustion.* 2000: Cambridge university press.
42. Pocheau, A. and F. Harambat, *Front propagation in a laminar cellular flow: Shapes, velocities, and least time criterion.* Physical Review E, 2008. **77**(3): p. 036304.
43. Poinsot, T., S. Candel, and A. Trouvé, *Applications of direct numerical simulation to premixed turbulent combustion.* Progress in Energy and Combustion Science, 1995. **21**(6): p. 531-576.
44. Sabel'Nikov, V., C. Corvellec, and P. Bruel, *Analysis of the influence of cold front quenching on the turbulent burning velocity associated with an eddy-break-up model.* Combustion and Flame, 1998. **113**(4): p. 492-497.
45. Sung, C., C. Sun, and C. Law, *Analytic description of the evolution of two-dimensional flame surfaces.* Combustion and Flame, 1996. **107**(1-2): p. 114-124.
46. Venkateswaran, P., A. Marshall, D.H. Shin, D. Noble, J. Seitzman, and T. Lieuwen, *Measurements and analysis of turbulent consumption speeds of H_2/CO mixtures.* Combustion and Flame, 2011. **158**(8): p. 1602-1614.
47. Venkateswaran, P., A. Marshall, J. Seitzman, and T. Lieuwen, *Turbulent consumption speeds of high hydrogen content fuels from 1-20 atm*, in *ASME Turbo Expo*2013: San Antonio, Texas, USA.
48. Venkateswaran, P., A. Marshall, J. Seitzman, and T. Lieuwen, *Pressure and fuel effects on turbulent consumption speeds of H_2/CO blends.* Proceedings of the Combustion Institute, 2013. **34**: p. 1527-1535.
49. Weinan, E., *Aubry–Mather theory and periodic solutions of the forced Burgers equation.* Comm. Pure Appl. Math, 1999. **52**(7): p. 811-828.
50. Wiggins, S., *Introduction to applied nonlinear dynamical systems and chaos.* 2nd ed. 2003: Springer.
51. Xin, J., *An Introduction to Fronts in Random Media.* Surveys and Tutorials in the Applied Mathematical Sciences (5). 2009.
52. Xin, J. and Y. Yu, *Analysis and Comparison of Large Time Front Speeds in Turbulent Combustion Models.* arXiv preprint, arXiv:1105.5607 [math.AP], 2011.
53. Xin, J. and Y. Yu. *Sharp asymptotic growth laws of turbulent flame speeds in cellular flows by inviscid Hamilton–Jacobi models.* in *Annales de l'Institut Henri Poincare (C) Non Linear Analysis.* 2013. Elsevier.
54. Yu, K., C. Sung, and C. Law, *Some aspects of the freely propagating premixed flame in a spatially periodic flow field.* Combustion and Flame, 1994. **97**(3-4): p. 375-383.
55. Zeldovich, I., G.I. Barenblatt, V. Librovich, and G. Makhviladze, *Mathematical Theory of Combustion and Explosions.* 1985, New York: Consultants Bureau (Plenum Publishing Corporation).